ZIBELINE INTERNATIONAL™ PUBLISHING

ISSN: 2716-5655 (Online)
CODEN: BDWRAP

Big Data in Water Resources Engineering (BDWRE)

DOI: http://doi.org/10.26480/bdwre.01.2025.01.06

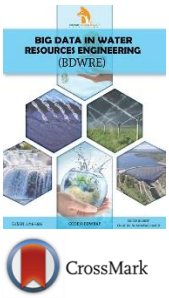

CrossMark

RESEARCH ARTICLE

APPLICATIONS OF DATA ANALYSIS PRINCIPLES FOR THE PREDICTION OF RESERVOIR QUALITY OF THE ELMA FIELD NIGER DELTA

Onome O. Okobiebi[a], Delik Celik[b], Kenneth Ojeaga[b*]

[a] Big Data and Data Science Technology, Northumbria University E17 HT London.
[b] Department of Science Laboratory Technology, University of Benin, PMB 1154 Ugbowo Benin City, Nigeria.
**Corresponding author's Email: kenneth.ojeaga@uniben.edu*

ARTICLE DETAILS

Article History:

Received 04 February 2025
Revised 20 March 2025
Accepted 25 April 2025
Available online 07 May 2025

ABSTRACT

This study investigates the application of data analysis on well-log data to ascertain the distribution of potential reservoir sands in the ELMA field Niger Delta. The data used for the analysis consists of the 14 wells that penetrated the ELMA field. The field consists of various lithologies interpreted from the core ranging from channel sands (CH), Lower Shoreface (LSF), Upper Shoreface (USF), Heterolith (HT) and Shales (SH). These Well data were cleaned and plotted using Python script and analysed using charts and tables to ascertain the percentage distribution of each facies in the field and the overall percentage of viable pay sands in the field. The analysis showed that the distribution of lithologies was 52.74% for SH, 22.69 for USF, 20.70 for CH, 2.75 for LSF and 1.11 HT. The overall net pay of the field was 47.3% which points to a high reservoir potential in the field with an accompanying possibility of sealing shale of 52.7%.

KEYWORDS

Reservoir, Pay zone, hydrocarbon, Logs, lithologies

1. INTRODUCTION

According to IBISWorld, the global economy relies significantly on the oil and gas sector, one of the largest industries worldwide. The upstream oil sector is the most important in the oil and gas industry, (Michael, 2018). The lithofacies identification during reservoir studies is the foundation of oil and gas exploitation when estimating reservoir properties, and conducting lithostratigraphic analysis (Li et al., 2020). It is carried out through physical observation of cores and the derivation of physical characteristics from the logs by geoscientists. Its identification forms the basic workflow of geoscientists in reservoir characteristics i.e. ascertaining the potential of the sands to hold fluid and precursor to property distribution in reservoir modelling (Madal and Rezaee 2019; Xiong, et al., 2010). This depositional environment exhibits the typical channel and shoreface deposits typical of the Niger Delta as described by various authors' research work by who described facies types like channel, upper shoreface, lower shoreface, heteroliths and shales from log motif analysis, patterns, and trends within the ELMA field (Okobiebi and Okobiebi, 2021). The present study is carried out to use data analysis to ascertain the distribution of the different lithologies and the net pay reservoir in the ELMA field.

1.1 Principles of facies Classification

The five major log trends in the Niger Delta for lithology identification (Figure 4) are log successions that gradually decrease in gamma-ray value (funnel shape) and then rapidly increase (gradually coarsen and then abruptly fine) and are interpreted to be prograding delta deposits. Those that abruptly decrease in gamma ray value and have "blocky" or gradually increasing trends i.e., bell shape (abruptly coarsen and remains sandy or gradually fine) are interpreted to be channel deposits, bow shape (systematic increase and decrease of gamma counts) and irregular trend (no systematic change in gamma values) (Cant, 1992).

2. METHODOLOGY

Data from the 14 wells in the field are in text format and were imported into IDE Jupyter and using the Pandas libraries. The data contains different logs These 14 files were then concatenated into a single combined file and analysed using the tables, histograms, boxplots, and charts.

2.1 Data Preprocessing

The wells contain logs like 'DEPT', 'CALI', 'DEN', 'FLD', 'GR', 'POR', 'RESDEP', 'RESMIC', 'RT', 'SH_AR', 'SH_WS', 'SW', 'SW_AR', 'TVDSS', 'VSH', 'Facies',' 'Zoneloglinkedto' 'Ahiatops_test', ''sequencestrat', 'P-zone', 'F-zone', 'MD', 'Permeability_total_BC', 'Permeability_total_HC', 'Permeability_total_LC', 'Porosity_total', 'RES_NET_FLAG_BC', 'RES_NET_FLAG_HC', 'RES_NET_FLAG_LC', 'Saturation'. Most of these logs were dropped to the necessarily needed logs. The 14 wells were pre-processed to ascertain the null data and outliers. Using lithofacies as the foundation of preprocessing all rows not containing lithology description were dropped as only real data sets are preferred for this analysis.

2.2 Well log displays

The well logs for the wells were displayed using the Python scripts for all Wells to give a general understanding of the lithology in the field. fig 1 to 9. This was used to visually observe the sand-to-shale ratio and the lithology type. The gamma-ray log is scaled from 0 – 150 API with the cut-off value of 75 API based on the maximum and minimum deflections observed from the Gamma Ray log which is the primary log for reservoir and non-reservoir detection as well as lithology type based on shapes. The different lithology was colour-coded using the colour code in Figure 1.

Quick Response Code	Access this article online	
	Website: www.bdwre.com.my	**DOI:** 10.26480/bdwre.01.2025.01.06

Cite The Article: Onome O. Okobiebi, Delik Celik, Kenneth Ojeaga (2025). Applications of Data Analysis Principles for The Prediction of Reservoir Quality of The Elma Field Niger Delta. *Big Data in Water Resources Engineering, 6(1): 01-06.*

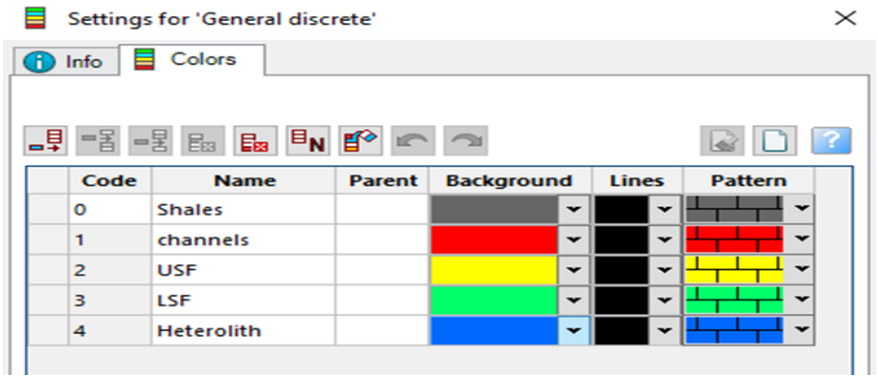

Figure 1: Showing the colour code for each sediment type.

2.3 Data Analysis

The analysis for the lithology type was carried out using tables, histograms, and pie charts. This was done to ascertain the reservoir quality of the field.

$$reservoir\ \% = \left(\frac{Reservoir}{Reservoir + Non{-}reservoir}\right) * 100 \quad (1)$$

3. Results and Discussion

The importation of the 14 wells was done on Jupyter Notebook and combined into one csv file as shown in Figure 2. Then preprocessing was done to remove all rows in the facies columns containing null data as shown in Figure 3. This affected wells ELMA-9, ELMA-10, ELMA-11, ELMA-12, and ELMA-14.

```
# Combine the two DataFrames vertically
combined_df = pd.concat([data1, data2, data3, data4, data5,data6,data7,data8,data9,data10,data11,data12,data13,data14], ignore_i
```

```
combined_df
```

```
combined_df.info()
```

```
<class 'pandas.core.frame.DataFrame'>
RangeIndex: 284993 entries, 0 to 284992
Data columns (total 8 columns):
 #   Column     Non-Null Count   Dtype
---  ------     --------------   -----
 0   DEPT       284993 non-null  float64
 1   GR         137433 non-null  float64
 2   SP         185006 non-null  float64
 3   DEN        191574 non-null  float64
 4   RESDEP     157650 non-null  float64
 5   Facies     132584 non-null  float64
 6   Well_name  284993 non-null  object
 7   POR        22551 non-null   float64
dtypes: float64(7), object(1)
memory usage: 17.4+ MB
```

```
# Save the combined DataFrame to a new CSV file
combined_df.to_csv('combined_file.csv', index=False)
```

```
combined_df.describe()
```

	DEPT	GR	SP	DEN	RESDEP	Facies	POR
count	284993.000000	137433.000000	1.850060e+05	191574.000000	157650.000000	132584.000000	22551.000000
mean	6121.225714	75.917487	-2.140893e+12	-3781.249699	21.414959	0.759775	0.214830
std	3370.370044	29.295701	9.200004e+14	4850.311670	64.383981	0.940652	0.112068
min	0.000000	-2.791200	-3.957134e+17	-9999.000000	0.000000	0.000000	0.036800
25%	3239.000000	49.706200	-9.999000e+03	-9999.000000	2.832050	0.000000	0.072000
50%	6375.500000	83.524597	3.392499e+01	2.234700	5.764900	0.000000	0.225900
75%	8920.000000	97.412003	6.274829e+01	2.450600	15.624975	2.000000	0.318000
max	13152.000000	272.250000	1.753600e+04	2.788714	8728.500977	4.000000	0.406000

Figure 2: Showing the codes that were used to concat the data frame for all the wells.

```
In [13]: data.isnull().sum()

Out[13]: Depth            0
         GR          147560
         SP           99987
         DEN          93419
         RESDEP      127343
         Facies      152409
         Well_name        0
         POR         262442
         lithofacies 152409
         dtype: int64
```

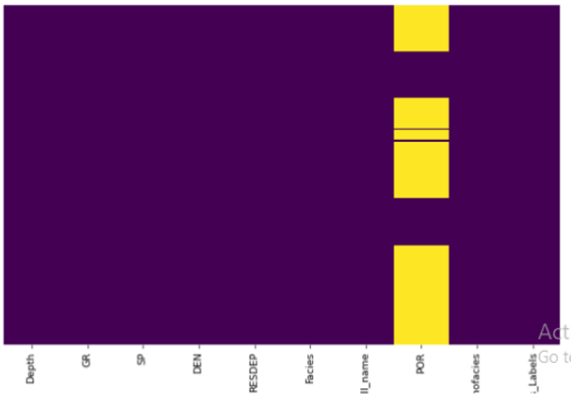

Figure 3: Showing the codes for dropping null data in facies and the resulting heat map.

The wells with facies logs were then displayed using tracks and sub-tracks. Figure 4 to Figure 6 shows the wells logs displayed for Well ELMA-1. Track 1 shows the Gamma-ray logs detect reservoir (sand) and non-reservoir sediments (shale). The yellow partition delineates sand, and the grey is shale. The second track with the blue line is the spontaneous potential (SP) log which also delineates sands and shale higher SP reading shows non-reservoir sands and the lower one depicts reservoir sand. The third track shows the density plot (DEN) and lastly, the fourth track shows the resistivity plot (RESDEP), and the last track depicts the different colour codes of the various lithology types in the field.

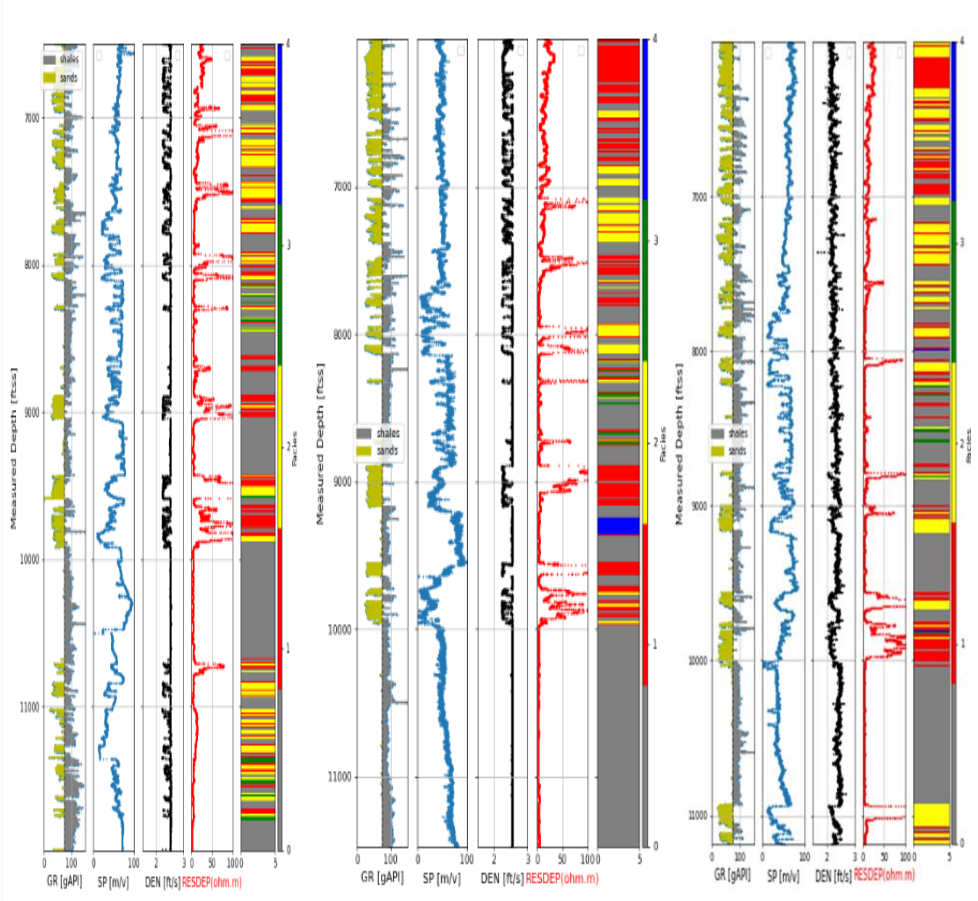

Figure 4: (a) Showing the well logs in ELMA-1 (b) Showing the wells logs in ELMA-2, (c) Showing the well logs in ELMA-3

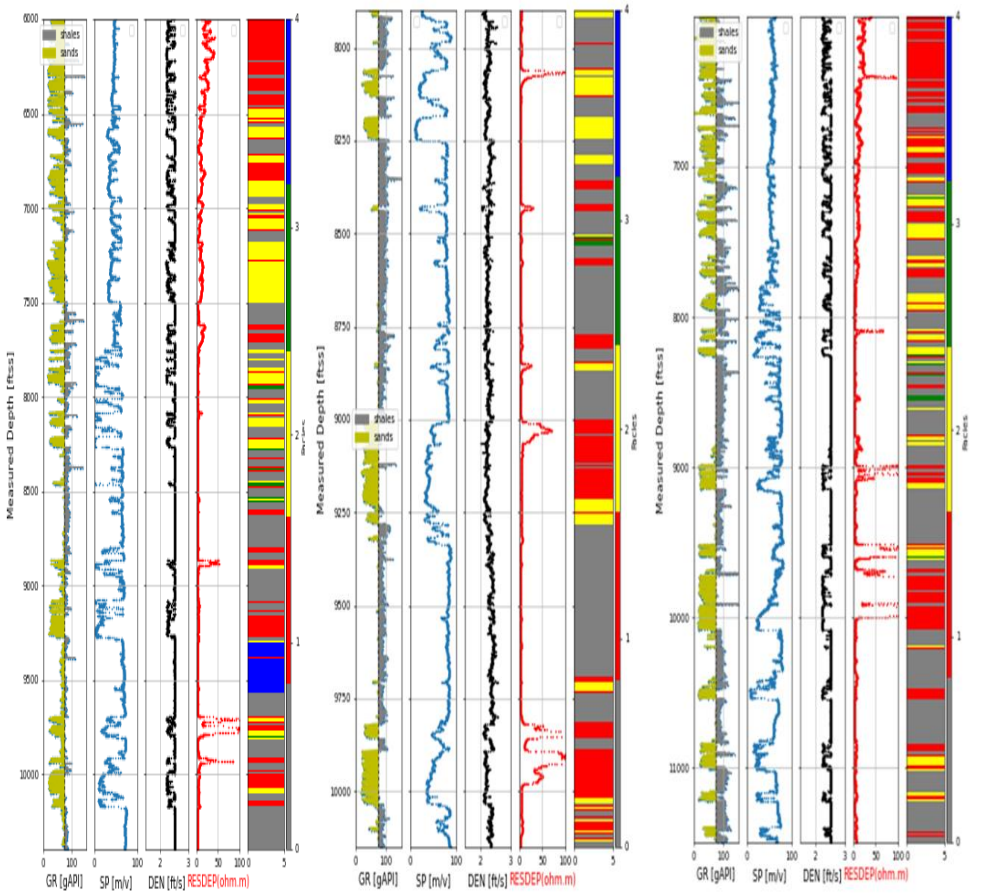

Figure 5: (a) Showing the wells logs in ELMA-4 (b) Showing the well logs in ELMA-5, (c) Showing the wells logs in ELMA-6

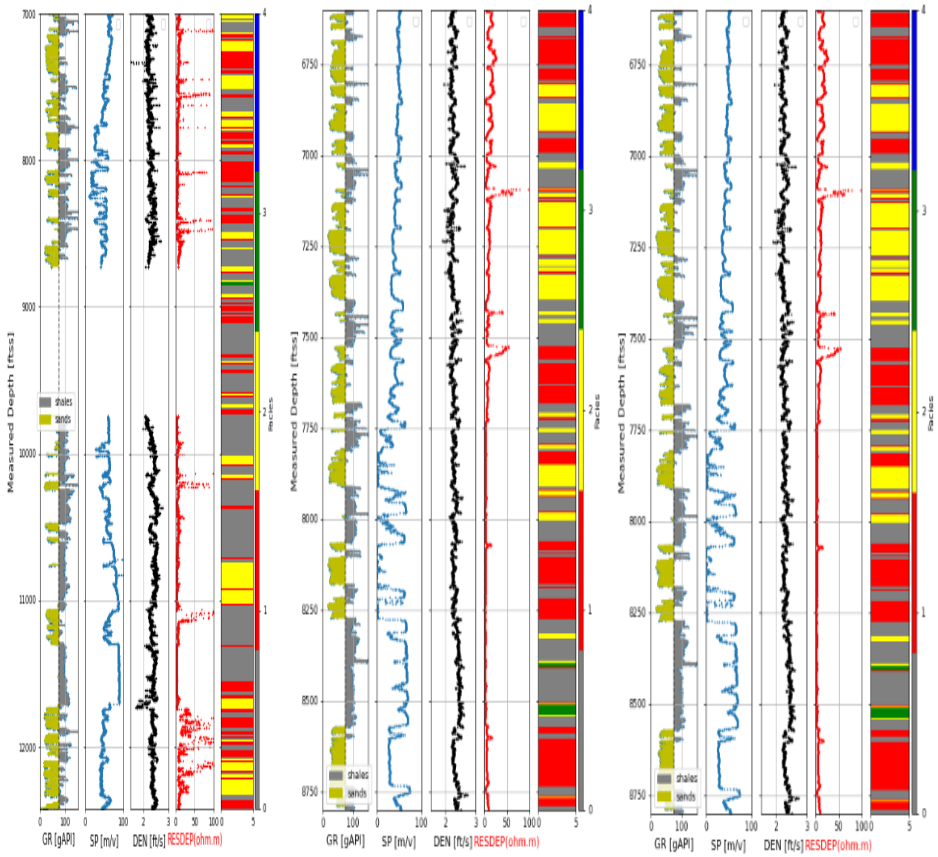

Figure 6: (a) Showing the well logs in ELMA-7 (b) Showing the wells logs in ELMA-8 (c) Showing the well logs in ELMA-13

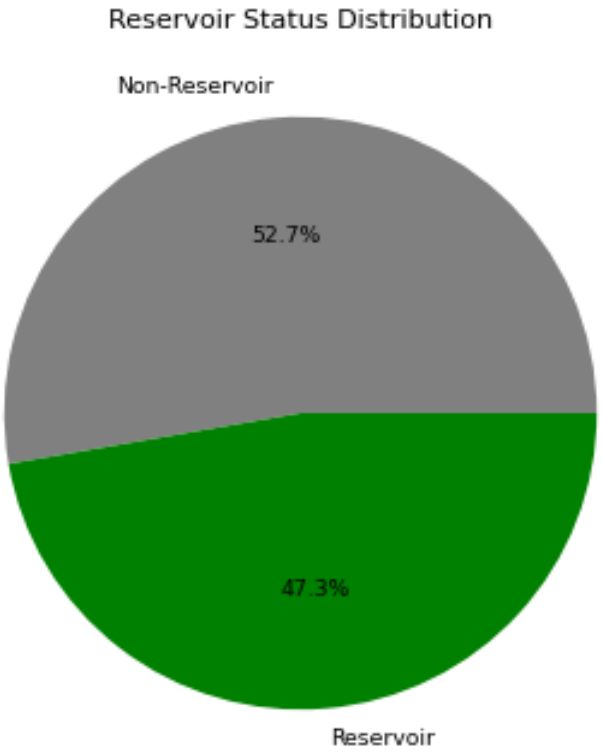

Figure 7: Showing the percentage of reservoir and non-reservoir sand.

The first analysis was done to ascertain the likelihood of reservoir formation in the field and a pie chart show was created from the dataset to ascertain the percentage of reservoir to non-reservoir sands in the ELMA field. The charts in Figure 7 showed that 52.7% of the penetrated lithology was non-reservoir sands and 47.7% was reservoir sand. This ratio is highly optimistic that there is a high chance of accumulation because Hydrocarbon reservoir sand that is thick enough, highly porous and permeable gives better prospects, higher volume and profit and as such, major Oil Companies indicate keen interest in such reservoir sands (Nduaguibe and Ideozu, 2019).

Data analysis was carried out on the 9 wells in the dataset, to ascertain the lithology types in the field. A histogram plot shows the percentage distribution of lithologies in the field, with the most dominant lithology being background marine shale which is about 52.74% of the total sediments package, 22.69% was upper shoreface, 20.70% were Channel deposits, 2.75% were Lower Shoreface deposits and 1.1% were Heterolith as shown in Figure 8. The is enlightens us on the quality of reservoir sands where studies shows that channels, upper shoreface have higher reservoir quality than that of lower shoreface and heterolith (Nduaguibe and Ideozu, 2019).

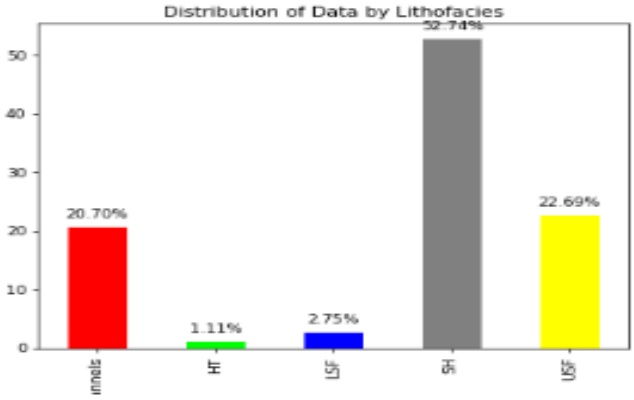

Figure 8: Distribution of the data by facies in the ELMA field. Note that the background SH (marine shale) facies occur significantly more than any other.

4. Conclusion

A satellite-based model known as METRIC is utilized to compute extraterrestrial temperature (ET) as a residual of energy balance at the surface of the Earth. The energy balance model developed by METRIC was implemented on the cropland site in Korea known as CFK. For the purpose of AET estimation, Landsat 9 images were retrieved for each of the ten different DOYs. The meteorological data from CFK were utilized as input components, and the flux data were utilized for the approval of the AET. In-situ flux data were used in the statistical analysis, and the results showed that METRIC has the potential to be an appropriate model for indirect AET estimation on a regional scale. Due to the fact that this model was developed for dry and semi-arid climates, it appears that some adjustments are still required in order to extend the applicability of the model. This is because there are some limitations in the assumptions that underlie the hot and cold pixel (i.e., a hot pixel has little to no ET, and a cold pixel has little to no H) when applied in a humid climate. When taken as a whole, these findings would be extremely helpful in the construction of effective water management and irrigation systems. The optimization of the dry/wet scaling, which isolates the performance of the model, should be improved for the purpose of further research. This will allow for a more precise application of the model in environments that are complex and full of various types of topography.

References

Alizadeh, O., 2022. Advances and challenges in climate modeling. Climatic Change, 170, Pp. 18.

Allen, R., Irmak, A., Trezza, R., Hendrickx, J.M., Bastiaanssen, W., Kjaersgaard, J., 2011a. Satellite-based ET estimation in agriculture using SEBAL and METRIC. Hydrological processes, 25, Pp. 4011-4027.

Allen, R.G., Pereira, L.S., Howell, T.A., Jensen, M.E., 2011b. Evapotranspiration information reporting: I. Factors governing measurement accuracy. Agricultural Water Management, 98, Pp. 899-920.

Allen, R.G., Tasumi, M., Morse, A., Trezza, R., Wright, J.L., Bastiaanssen, W., 2007a. Satellite-based energy balance for mapping evapotranspiration with internalized calibration (METRIC)—Applications. Journal of irrigation and drainage engineering, 133, Pp. 395-406.

Allen, R.G., Tasumi, M., Trezza, R., 2007b. Satellite-based energy balance for mapping evapotranspiration with internalized calibration (METRIC)—Model. Journal of irrigation and drainage engineering, 133, Pp. 380-394.

Aslam, M., Arshad, M., Hussain, S., Usman, M., Zahid, M.B., Sattar, J., 2021. An integrated approach for estimation of van genuchten model parameters in undisturbed and unsaturated soils. Pakistan Journal of Agricultural Sciences, Pp. 58.

Awada, H., Di Prima, S., Sirca, C., Giadrossich, F., Marras, S., Spano, D., 2022. A remote sensing and modeling integrated approach for constructing continuous time series of daily actual evapotranspiration. Agricultural Water Management, 260, Pp. 107320.

Baeumler, N.W., Kjaersgaard, J., Gupta, S.C., 2019. Evapotranspiration from corn, soybean, and prairie grasses using the METRIC model. Agronomy Journal, 111, Pp. 770-780.

Bales, R.C., Molotch, N.P., Painter, T.H., Dettinger, M.D., Rice, R., Dozier, J., 2006. Mountain hydrology of the western United States. Water Resources Research, Pp. 42.

Bastiaanssen, W., Noordman, E., Pelgrum, H., Davids, G., Thoreson, B., Allen, R., 2005. SEBAL model with remotely sensed data to improve water-resources management under actual field conditions. Journal of irrigation and drainage engineering, 131, Pp. 85-93.

Cai, W., Ullah, S., Yan, L., Lin, Y., 2021. Remote sensing of ecosystem water use efficiency: a review of direct and indirect estimation methods. Remote Sensing, 13, Pp. 2393.

Chandole, V., Joshi, G.S., Rana, S.C., 2019. Spatio-temporal trend detection of hydro-meteorological parameters for climate change assessment in Lower Tapi river basin of Gujarat state, India. Journal of Atmospheric and Solar-Terrestrial Physics, 195, Pp. 105130.

Cheema, M.J.M., Iqbal, T., Daccache, A., Hussain, S., Awais, M., 2023. Precision agriculture technologies: Present adoption and future strategies. Precision Agriculture. Elsevier, Pp. 231-250.

Chen, X., Su, Z., Ma, Y., Trigo, I., Gentine, P., 2021. Remote sensing of global daily evapotranspiration based on a surface energy balance method and reanalysis data. Journal of Geophysical Research: Atmospheres, 126, Pp. e2020JD032873.

Chen, X., van der Werf, J.A., Droste, A., Coenders-Gerrits, M., Uijlenhoet, R., 2025. Barriers of urban hydro-meteorological simulation: a review. EGUsphere, Pp. 1-48.

Demuzere, M., Kittner, J., Martilli, A., Mills, G., Moede, C., Stewart, I.D., 2022. A global map of Local Climate Zones to support earth system modelling and urban scale environmental science. Earth System Science Data Discussions, Pp. 1-57.

Derardja, B., Khadra, R., Abdelmoneim, A.A.A., El-Shirbeny, M.A., Valsamidis, T., De Pasquale, V., 2024. Advancements in Remote Sensing for Evapotranspiration Estimation: A Comprehensive Review of Temperature-Based Models. Remote Sensing, 16, Pp. 1927.

Dhungel, S., Barber, M.E., 2018. Estimating calibration variability in evapotranspiration derived from a satellite-based energy balance model. Remote sensing, 10, Pp. 1695.

Feng, H., Wang, S., Zou, B., Nie, Y., Ye, S., Ding, Y., 2023. Land use and cover change (LUCC) impacts on Earth's eco-environments: Research progress and prospects. Advances in Space Research, 71, Pp. 1418-1435.

Foken, T., Leuning, R., Oncley, S.R., Mauder, M., Aubinet, M., 2012. Corrections and data quality control. Eddy covariance: a practical guide to measurement and data analysis, Pp. 85-131.

Foolad, F., Blankenau, P., Kilic, A., Allen, R.G., Huntington, J.L., Erickson, T.A., 2018. Comparison of the automatically calibrated Google Evapotranspiration Application—EEFlux and the manually calibrated METRIC application.

Fugger, S., Shaw, T.E., Jouberton, A., Miles, E.S., Buri, P., McCarthy, M., 2024. Hydrological regimes and evaporative flux partitioning at the climatic ends of high mountain Asia. Environmental Research Letters, 19, Pp. 044057.

García-Santos, V., Sánchez, J.M., Cuxart, J., 2022. Evapotranspiration acquired with remote sensing thermal-based algorithms: a state-of-the-art review. Remote Sensing, 14, Pp. 3440.

Hadadi, F., Moazenzadeh, R., Mohammadi, B., 2022. Estimation of actual evapotranspiration: A novel hybrid method based on remote sensing and artificial intelligence. Journal of Hydrology, 609, Pp. 127774.

Hussain, S., Malik, S., Masud Cheema, M., Ashraf, M.U., Waqas, M., Iqbal, M., 2020. An overview on emerging water scarcity challenge in Pakistan, its consumption, causes, impacts and remedial measures. Big Data in Water Resources Engineering, 1, Pp. 22-31.

Iqbal, M.M., Hussain, S., Cheema, M., Jehanzeb, M., Lee, J.L., Waqas, M.S., 2022a. Seasonal effect of agricultural pollutants on coastline environment: a case study of the southern estuarine water ecosystem of the boseong county Korea. Pakistan Journal of Agricultural Sciences, Pp. 59.

Iqbal, M.M., Li, L., Hussain, S., Lee, J.L., Mumtaz, F., Elbeltagi, A., 2022b. Analysis of seasonal variations in surface water quality over wet and dry regions. Water, 14, Pp. 1058.

Iqbal, M.M., Shoaib, M., Agwanda, P.O., 2019. The response of pollution load from coastal river waterfront on red tides in South Sea. Journal of Coastal Research, 91, Pp. 231-235.

Iqbal, M.M., Shoaib, M., Farid, H.U., Lee, J.L., 2018. Assessment of water quality profile using numerical modeling approach in major climate classes of Asia. International journal of environmental research and public health, 15, Pp. 2258.

Irmak, A., Allen, R.G., Kjaersgaard, J., Huntington, J., Kamble, B., Trezza, R., 2012. Operational remote sensing of ET and challenges. Evapotranspiration—Remote Sensing and Modeling, Pp. 467-492.

Kjaersgaard, J., Allen, R., Irmak, A., 2011. Improved methods for estimating monthly and growing season ET using METRIC applied to moderate resolution satellite imagery. Hydrological Processes, 25, Pp. 4028-4036.

Knowles, J.F., Burns, S.P., Blanken, P.D., Monson, R.K., 2015. Fluxes of energy, water, and carbon dioxide from mountain ecosystems at Niwot Ridge, Colorado. Plant Ecology and Diversity, 8, Pp. 663-676.

Li, J., Miao, C., Wei, W., Zhang, G., Hua, L., Chen, Y., 2021. Evaluation of CMIP6 global climate models for simulating land surface energy and water fluxes during 1979–2014. Journal of Advances in Modeling Earth Systems, Pp. 13: e2021MS002515.

Li, M.,. Peng, J., Lu, Z., Zhu, P., 2023a. Research progress on carbon sources and sinks of farmland ecosystems. Resources, Environment and Sustainability, 11, Pp. 100099.

Li, Z.L., Wu, H., Duan, S.B., Zhao, W., Ren, H., Liu, X., 2023b. Satellite remote sensing of global land surface temperature: Definition, methods, products, and applications. Reviews of Geophysics, Pp. 61.

Liou, Y.A., Kar, S.K., 2014. Evapotranspiration estimation with remote sensing and various surface energy balance algorithms—A review. Energies, 7, Pp. 2821-2849.

Marmy, A., Rajczak, J., Delaloye, R., Hilbich, C., Hoelzle, M., Kotlarski, S., 2016. Semi-automated calibration method for modelling of mountain permafrost evolution in Switzerland. The Cryosphere, 10, Pp. 2693-2719.

Massman, W., Finnigan, J., Billesbach, D., Miller, S., Black, A., Amiro, B., 2003. Summary and synthesis of recommendations of the AmeriFlux Workshop on standardization of flux analysis and diagnostics; Corvallis, Oregon; August 2002. Oak Ridge, TN: Oak Ridge National Laboratory, AmeriFlux Network, AmeriFlux Workshop Team. Online: http://public. ornl. gov/ameriflux/workshops/workshop-20020827-corvallisOR-summary. doc, 2003.

Mauder, M., Foken, T., Clement, R., Elbers, J.A., Eugster, W., Grünwald, T., 2008. Quality control of CarboEurope flux data–Part 2: Inter-comparison of eddy-covariance software. Biogeosciences, 5, Pp. 451-462.

Mazhar Iqba, M., Abid, I., Hussain, S., Shahzad, N., Sohail Waqas, M., Jawed Iqbal, M., 2020. The effects of regional climatic condition on the spread of COVID-19 at global scale.

Novick, K., Walker, J., Chan, W., Schmidt, A., Sobek, C., Vose, J., 2013. Eddy covariance measurements with a new fast-response, enclosed-path analyzer: Spectral characteristics and cross-system comparisons. Agricultural and Forest Meteorology, 181, Pp. 17-32.

Pongratz, J., Schwingshackl, C., Bultan, S., Obermeier, W., Havermann, F., Guo, S., 2021. Land use effects on climate: current state, recent progress, and emerging topics. Current Climate Change Reports, Pp. 1-22.

Rebmann, C., Kolle, O., Heinesch, B., Queck, R., Ibrom, A., Aubinet, M., 2012. Data acquisition and flux calculations. Eddy covariance: a practical guide to measurement and data analysis, Pp. 59-83.

Reyes-González, A., Kjaersgaard, J., Trooien, T., Hay, C., Ahiablame, L., 2017. Comparative analysis of METRIC model and atmometer methods for estimating actual evapotranspiration. International Journal of Agronomy, Pp. 3632501.

Rezaei, M., Ghasemieh, H., Abdollahi, K., 2021. Simplified Version of the METRIC Model for Estimation of Actual Evapotranspiration. International Journal of Remote Sensing, 42, Pp. 5568-5599.

Runkle, B.R., Wille, C., Gažovič, M., Kutzbach, L., 2012. Attenuation correction procedures for water vapour fluxes from closed-path eddy-covariance systems. Boundary-layer meteorology, 142, Pp. 401-423.

Senay, G.B., Budde, M.E., Verdin, J.P., 2011. Enhancing the Simplified Surface Energy Balance (SSEB) approach for estimating landscape ET: Validation with the METRIC model. Agricultural Water Management, 98, Pp. 606-618.

Shuttleworth, W.J., 2012. Terrestrial hydrometeorology: John Wiley & Sons.

Song, L., Ding, Z., Kustas, W.P., Xu, Y., Zhao, G., Liu, S., 2022. Applications of a thermal-based two-source energy balance model coupled to surface soil moisture. Remote Sensing of Environment, 271, Pp. 112923.

Sun, Y., Ding, L., Su, B., Dowsett, H., Wu, H., Hu, J., 2024. Modeling the mid-piacenzian warm climate using the water isotope-enabled Community Earth System Model (iCESM1. 2-ITPCAS). Climate Dynamics, 62, Pp. 7741-7761.

Trezza, R., Allen, R.G., Tasumi, M., 2013. Estimation of actual evapotranspiration along the Middle Rio Grande of New Mexico using MODIS and landsat imagery with the METRIC model. Remote Sensing, 5, Pp. 5397-5423.

Waqas, M.S., Cheema, M.J.M., Hussain, S., Ullah, M.K., Iqbal, M.M., 2021. Delayed irrigation: An approach to enhance crop water productivity and to investigate its effects on potato yield and growth parameters. Agricultural Water Management, 245, Pp. 106576.

Waqas, M.S., Cheema, M.J.M., Waqas, A., Hussain, S., 2018. Enhancing water productivity of potato (Solanum tuberosum L.) through drip irrigation system. Proceedings of Pakistan Society for Horticultural Science, Pp. 18-20.

Xu, F., Fan, J., Yang, C., Liu, J., Zhang, X., 2022. Reconstructing all-weather daytime land surface temperature based on energy balance considering the cloud radiative effect. Atmospheric Research, 279, Pp. 106397.

Xue, X., Jin, S., An, F., Zhang, H., Fan, J., Eichhorn, M.P., 2022. Shortwave radiation calculation for forest plots using airborne LiDAR data and computer graphics. Plant Phenomics.

Yang, Y., Roderick, M.L., 2019. Radiation, surface temperature and evaporation over wet surfaces. Quarterly Journal of the Royal Meteorological Society, 145, Pp. 1118-1129.

Zhang, Q., Zhang, Y., Yu, T., Zhong, D., 2024. Primary driving factors of ecological environment system change based on directed weighted network illustrating with the Three-River Headwaters Region. Science of The Total Environment, 916, Pp. 170055.

Zhu, S., Causone, F., Gao, N., Ye, Y., Jin, X., Zhou, X., 2023. Numerical simulation to assess the impact of urban green infrastructure on building energy use: A review. Building and Environment, 228, Pp. 109832.